

# Ice - Ocean Interactions underneath the Antarctic Ice Shelf Ekströmisen

by Marcel Nicolaus<sup>1</sup> and Klaus Grosfeld<sup>2</sup>

**Abstract:** We applied a three-dimensional ocean circulation model to the cavity underneath Ekströmisen, one of the eastern Weddell ice shelves, and the adjacent open ocean. The main objective of this study is to describe ice-ocean interactions and resulting freshwater fluxes within the cavity and their contribution to the thermohaline driving forces of the Coastal Current. This study is characterized by temporally and spatially high resolution analyses of circulation patterns, basal melt rates and water mass configurations as well as their seasonal variations. To achieve these aims, new geometric data sets of water column thickness and ice shelf draft are compiled for the region. The vertically integrated mass transport within the model domain is dominated by a 0.6 Sv cyclonic gyre, which spans from the western part of the cavity onto the shelf region in front of the ice shelf. The resulting mass transport is partly driven by an ice pump process, which is related to an average mass loss of  $0.98 \text{ m}_{\text{ice}} \text{ a}^{-1}$  at the ice shelf base. No accretion of marine ice has been found. The narrow continental shelf permits a strong interaction with the Coastal Current and associated heat transports into the ice shelf cavity. Sensitivity studies with artificially extended continental shelves indicate the importance of precise and high resolution geometries in numerical models, especially in key regions as across the narrow continental shelf. An extension of the shelf width by only 11 km reduces the basal melt rate in the cavity by approximately 30 %, causing warmer and saltier water masses in the outflow. Color tracer experiments, visualizing the temporal variations of the flow regime, help to distinguish and locate seasonally varying source regions of water masses, penetrating into the ice shelf cavity and providing strong ice shelf-ocean interactions.

**Zusammenfassung:** Mit Hilfe eines dreidimensionalen Ozeanzirkulationsmodells wurde der Wassermassenaustausch und -transport in der Kaverne unter dem Ekströmisen, einem Schelfeisgebiet im östlichen Weddellmeer, und dem angrenzenden offenen Ozean simuliert. Ziel dieser Untersuchung ist die Quantifizierung der Schelfeis-Ozean-Wechselwirkungen und der daraus resultierende glaziale Süßwasserfluss innerhalb der Schelfeiskaverne und sein Beitrag für den thermohalinen Antrieb des Küstenstroms. Diese Studie zeichnet sich durch räumlich und zeitlich hoch aufgelöste Analysen von Zirkulationsmustern, basalen Schmelzraten und Wassermassen-Zusammensetzungen sowie deren saisonalen Veränderungen aus. Voraussetzung hierfür sind geometrische Datensätze der Wassersäulen-Mächtigkeit und des Schelfeis-Tiefgangs, die für diese Region aus verschiedenen Datensätzen zusammengestellt worden sind. Der vertikal integrierte Massentransport innerhalb der Modellregion des Ekströmisen wird von einem 0,6 Sv starken zyklonalen Wirbel dominiert, der sich aus der westlichen Kaverne bis auf den angrenzenden Kontinentalschelf erstreckt. Der resultierende glaziale Süßwasserfluss wird teilweise durch den Eispumpen-Prozess angetrieben, der einen mittleren Massenverlust von  $0,98 \text{ m}_{\text{eis}} \text{ a}^{-1}$  an der Schelfeis-Unterseite hervorruft. Es konnte keine Ablagerung marinen Eises in den Simulationsergebnissen beobachtet werden. Der enge Kontinentalschelf erlaubt eine starke Wechselwirkung mit dem Küstenstrom und dem mit ihm assoziierten Wärmetransport in die Schelfeiskaverne. Sensitivitätsstudien zum Einfluss der Kontinentalschelf-Breite auf die Durchströmung der Schelfeiskaverne heben die Bedeutung von genauen und hoch aufgelösten Geometrien in numerischen Modellen hervor. Bei einem künstlich um 11 km verbreiterten Kontinentalschelf reduziert sich die basale Schmelzrate in der Kaverne um ungefähr 30 %, was zu wärmeren und salzhaltigeren Wassermassen im Ausstrombereich führt. Experimente mit künstlichen Farbtacern dienen der Visualisierung von zeitlichen Veränderungen des Strömungsmusters, was unter anderem zur Unterscheidung und Lokalisierung von saisonal veränderlichen Quellregionen derjenigen Wassermassen führt, die in die Schelfeiskaverne einströmen und zur starken Wechselwirkung zwischen Schelfeis und Ozean beitragen.

## INTRODUCTION

About 44 % of the Antarctic coastline is fringed by ice shelves, which connect the inland ice sheet to the Southern Ocean. Due to iceberg calving and basal melting, ice shelves provide significant amounts of freshwater to the global ocean and complement beside other processes the net precipitation (P-E) fluxes (BECKMANN & GOOSSE 2003). The freshwater budget plays an important role for oceanic water mass transformations and deep water formation in the Southern Ocean (TIMMERMANN et al. 2001).

The most significant water mass modifications, in terms of cold and fresh Ice Shelf Water (ISW) entries, take place in the Weddell Sea region (FAHRBACH et al. 1994). Beside the large Filchner-Ronne Ice Shelf (FRIS) and Larsen Ice Shelves (LIS) the eastern Weddell Ice Shelves (EWIS) are contributing to this process by entering cold and fresh water into the Coastal Current. According to TIMMERMANN et al. (2001) 9.1 mSv ( $1 \text{ mSv} = 10^3 \text{ m}^3 \text{ s}^{-1}$ ) originating from ice-shelf basal melting and 19 mSv of net precipitation contribute to the freshwater balance in the inner Weddell Sea.

The region under investigation, the Ekströmisen, is part of the EWIS and is adjoining to Dronning Maude Land between  $10^\circ \text{W}$  and  $6^\circ \text{W}$ . A general topographic map is presented in Figure 1. Ekströmisen represents the logistic base for expeditions into the hinterland and accommodates the German wintering over base Neumayer Station. The Southern Ocean in this region is characterized by an extremely narrow continental shelf, enabling the close and strong Coastal Current to flow underneath the ice shelf through depressions or troughs in the sea bottom relief, leading to extensive ice shelf-ocean interactions. Depending on season, different water masses penetrate into the ice shelf cavity, whereas their  $\Theta$ S-characteristics are influenced through the sea ice coverage on the continental shelf (MARCUS et al. 1998).

The process of ice-shelf – ocean interaction and its impact on the hydrography can only be measured directly with enormous logistic efforts by means of hot water drillings and the installation of under ice moorings (e.g., MAKINSON 1994, ROBINSON et al. 1994, NICHOLLS & MAKINSON 1998). With this technique, NIXDORF et al. (1994) found seasonally varying basal melt rates close to the Ekströmisen ice front. In addition, measurements of hydrographic cross sections in front of ice shelves yield indications of water masses, influenced by ice shelf basal melting (e.g. FOLDVIK et al. 1985, PIATKOWSKI 1987, GAMMELSRØD et al. 1994). However, all these techniques do not derive a detailed areal distribution of basal melting and freezing rates and, hence, of the net fresh-water flux to the

<sup>1</sup> Alfred Wegener Institute for Polar and Marine Research, PO Box 120161, D-27515 Bremerhaven, Germany; <mnicolaus@awi-bremerhaven.de>.

<sup>2</sup> Department of Geosciences/MARUM, Bremen University, PO Box 330440, D-28334 Bremen, Germany; <grosfeld@palmod.uni-bremen.de>.

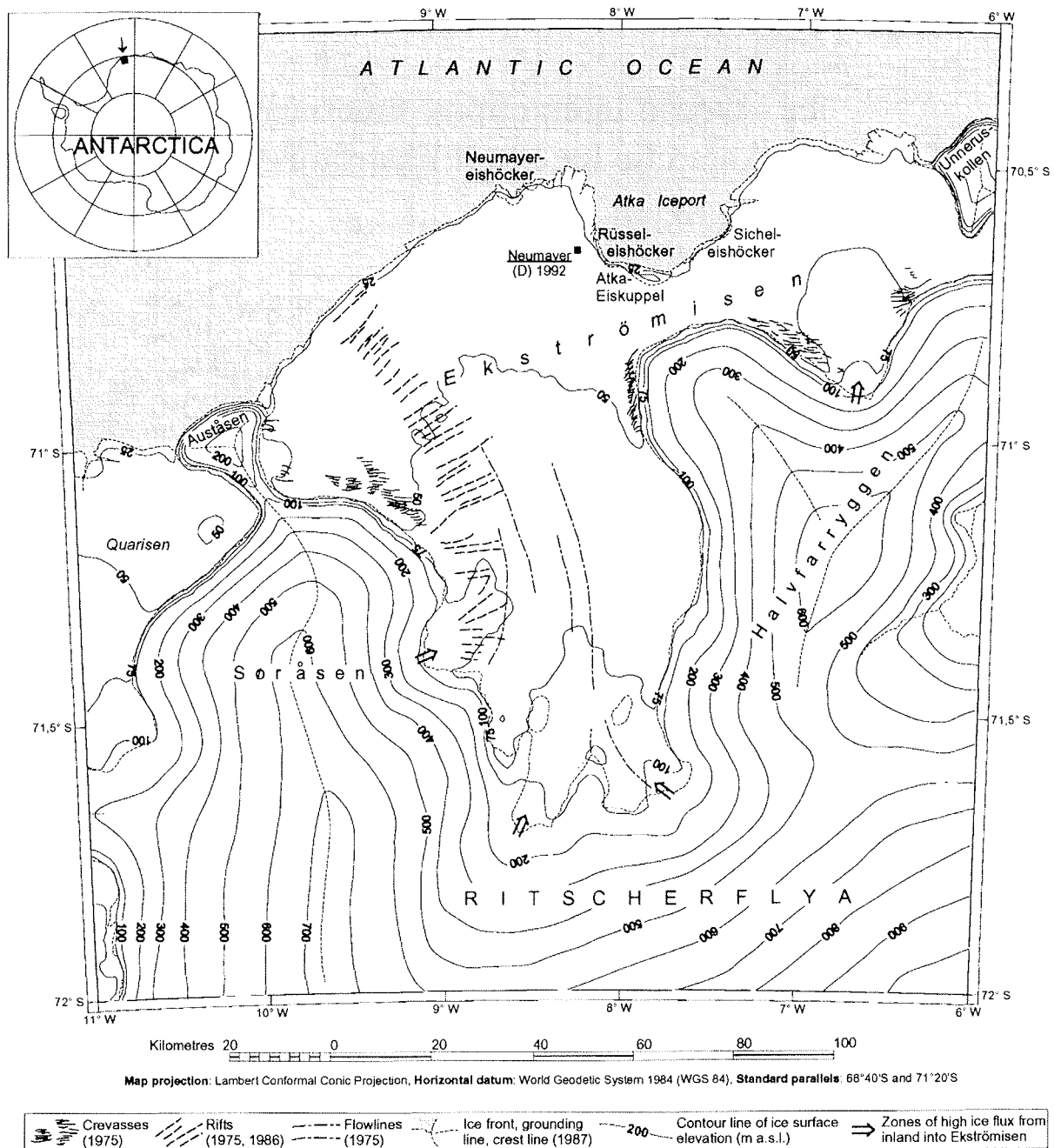


**Fig. 1:** General topographic map of Ekströmsen and the adjacent ice sheet and ice-shelf regions. Surface elevation is given in metres. Arrows mark the four main zones of ice flux from the inland into the ice shelf. Furthermore, the position of Neumayer Station and Atka ice rumples ("Atka-Eiskuppel") are labelled (from MÜLLER et al. 1997).

**Abb. 1:** Topographische Übersichtskarte des Ekströmsen und seiner angrenzenden Inland- und Schelfeisgebiete. Die Oberflächenhöhen sind in Meter angegeben. Pfeile markieren die vier Hauptzuflussgebiete von Eis aus dem Inland in das Schelfeis. Außerdem sind die Positionen der Neumayer-Station und der Atka-Eiskuppel angegeben (aus MÜLLER et al. 1997).

ocean. This is only possible by means of numerical modelling studies, which simulate the full oceanic flow regime and the corresponding process of ice-shelf – ocean interactions for given boundary conditions (e.g., BECKMANN et al. 1999, GERDES et al. 1999, WILLIAMS et al. 2001, JENKINS et al. 2002, HOLLAND et al. 2003).

Our study is, therefore, focused on the numerical simulation of the oceanic flow regime in the ice-shelf cavity, the basal mass

balance and resulting fresh water fluxes of the Ekströmsen, and its seasonal variations. The paper is structured as follows: in Section 2 the numerical model and the geometric setting are described. Section 3 shows the principal results of the control experiment, while in Sections 4 and 5 sensitivity studies according to the influence of the continental shelf widths are discussed. In Section 6 the influence of seasonality onto the mass balance is derived and Section 7 comprises a summary and conclusion of the main findings.

## NUMERICAL REALIZATION

As already stated above, it is not currently possible to extensively measure various water mass properties directly underneath ice shelves. Therefore, numerical models are applied which consider most physical processes as realistic as possible, to simulate oceanographic conditions in three dimensions with desired resolution. Furthermore, field measurements are included as initial and boundary conditions in this study to achieve even more realistic results.

### *General model description*

The three-dimensional thermohaline circulation model is based on a version of an Ocean General Circulation Model (OGCM) (BRYAN 1969, COX 1984) discretized horizontally in spherical coordinates. One of the main advantages of this model approach is that it permits a sufficiently high resolution of  $0.1^\circ$  (zonal)  $\cdot$   $0.05^\circ$  (meridional), necessary to reach adequate discretization within the cavity and across the continental shelf. Furthermore, the algorithm does not lose vertical resolution over shallow coastal regimes because terrain following  $\sigma$ -coordinates ( $\sigma$  = local depth / water column height) are used in the vertical plane. Layer thicknesses under the ice shelf range from 0.022 % (topmost layer) to 22.6 % (bottom layer) of the total water column to reinforce the predominance of near surface processes. In front of the ice shelf, four additional upper layers, each a quarter of the ice front thickness, are introduced. The model domain is discretized in finite differences and all variables are arranged on a Arakawa B grid (ARAKAWA 1966). In the time domain, an explicit stepping of 750 s (up to 80 % Courant-Friedrich-Lewy criterion) is used.

The model domain comprises the ice shelf cavity and the adjacent open ocean. Ice-ocean interaction underneath a realistic ice front allows a study of inflow/outflow of water masses into/from the cavity. Model integration starts from the ocean at rest and continues until a quasi steady state is reached after eight model years. The model is initialized with temperature and salinity values at all grid cells (see below). It predicts the horizontal velocity components, potential temperature and salinity on all  $\sigma$ -levels. The vertical velocity component  $w$ , perpendicular to the  $\sigma$ -surfaces, is a diagnostic variable calculated from continuity equation. Density is derived from the equation of state according to MELLOR (1991). A more detailed description of the model is given by GERDES (1993), GROSFELD et al. (1997), and GERDES et al. (1999).

The normal velocity component vanishes ( $v \cdot n = 0$ ) along all boundaries, and the model does not support any flow into or out of the model domain parallel to the coast. This disadvantage causes an artificial recirculation within the model domain which is described and discussed below. The implementation of more realistic boundary conditions to prescribe the natural Coastal Current (eastern inflow and western outflow parallel to the coast) is beyond this application of the model. The distribution of additional passive tracers, e.g. color injections, can be predicted to illustrate the modelled flow regime.

### *Ice-ocean interaction*

The ice shelf base represents the interface between sea water and meteoric ice. Considering these two sub-systems, thermodynamic exchange processes at this boundary have to be specified. In the model the ice shelf front acts as a passive interface where no melting or freezing occurs, because its contribution occurs mainly due to iceberg calving, which is neglected here. In addition, the area along the ice front (ice front height of 80 m times length of the ice front) is small compared to the area of one grid point exposed to basal melting and, therefore, the freshwater impact due to melting at the ice front is neglected.

Thermohaline processes in the sub-ice shelf cavity are based on a parameterization of the in situ freezing / melting point (FOLDVIK & KVINGE 1974). The predominance of pressure (related to depth) in this formulation becomes obvious by comparing the surface freezing point (about  $-1.9^\circ\text{C}$ , depending on salinity) with the freezing point at 1000 m depth, being  $0.7^\circ\text{C}$  lower. The resulting ice melt at the grounding line due to the presence of warm water masses, the meltwater buoyancy along the ascending ice shelf base, and the accretion of marine ice at shallower depth have first been described by ROBIN (1979) and referred to as the "ice pump" process by LEWIS & PERKIN (1986).

As a second fundamental equation an energy balance at the ice – ocean boundary is given (HELLMER & OLBERS 1989). With this, heat fluxes from the ocean directed into the ice and latent heat fluxes at the interface between the two systems are related. Furthermore, a salt balance is computed, whereby fluxes into the ice are neglected. Coupling these equations, the local melting temperature and the according basal melt rate can be determined. To parameterize heat and salt transfer at the ice – ocean boundary, a velocity dependent turbulent transfer coefficient is used (JENKINS 1991). The salt balance at the ice shelf base induces transport processes which affect the stratification of the water body, because salinity is the predominating quantity in the equation of state (MELLOR 1991). This is also remarkable at the ocean's surface where seasonal melting of sea ice and freezing of water occurs.

### *Geometric setting*

Ekströmisen is located between  $10.00^\circ\text{W}$  and  $6.25^\circ\text{W}$  and between  $71.75^\circ\text{S}$  and  $70.30^\circ\text{S}$  (Fig. 1). It covers an area of  $8700\text{ km}^2$  and is divided into a  $6700\text{ km}^2$  western and a smaller eastern part ( $2000\text{ km}^2$ ) (IFAG 1989). For the control experiment the model area spans  $71 \cdot 41$  grid cells, while an expanded ocean domain involves  $71 \cdot 71$  nodes (shelf00).

Two data sets are necessary to describe the model domain, the ice shelf draft and the sea floor topography. The difference between the constituent values is the water column thickness, which influences the ocean circulation. The ice shelf bottom geometry is based on Radio Echo Sounding (RES) measurements analyzed by SANDHÄGER & BLINDOW (2000) and is regridded from originally  $725\text{ m} \cdot 725\text{ m}$  to the model grid ( $3.4\text{ km}$  to  $4.2\text{ km}$  zonally, depending on latitude;  $5.6\text{ km}$  meridionally). The sea floor topography is taken from the General Bathymetric Chart of the Oceans (GEBCO) (IOC et al. 1997) and interpolated to the same grid. Hence, a high resolution

data set of Ekströmsen and the adjacent ocean is given, comprising sea floor depth, ice-shelf draft as well as water column thickness. It might serve as a geometric data base for future investigations on different scales and objectives.

Because the model demands an ice front position parallel to constant latitude, it is necessary to rotate the whole model domain 40° clockwise, adjusting the mean disorientation of the ice shelf front. Figure 2 shows the resulting water column thickness for the model domain. The geometry of the control experiment includes the ice shelf and ends beyond the narrow continental margin of about 35 km (at  $j = 41$ , Fig. 2 white dashed line). To underline this abrupt change toward deep-sea conditions it might be reflected that the continental shelf in front of the FRIS spans over about 500 km (SCHENKE 1997).

The maximum water column thickness underneath the ice shelf exceeds 500 m at the central depression of the sea floor, whereas a minimum of 50 m is set to guarantee a sufficient extension of the uppermost thin layers. Within the open ocean up to 4500 m water depth are reached. Due to increasing flow velocities of the ice shelf from south to north, the shelf-ice body itself is thinning from 760 m at the adjoining ice streams to 160 m towards the ice edge. The Atka ice rumples area, where the ice shelf is grounded, is treated as an island, such that no ice – ocean interaction occurs.

### Initialization and restoring

As described above, the ocean model is initialized with temperature and salinity values after ZWIERZ (1993) at each grid point at the beginning of model integration. Several parameter studies showed that different initializations converge towards the same steady state model years, hence they are not discussed here. Beside the prescription of initial values, further restoring profiles at the northern model boundary and at the open ocean's surface are needed to avoid a model drift due to permanent freshwater injections. Therefore, actual temperature and salinity values at the northern boundary ( $j = 41$ , and for later experiments at  $j = 71$ ) are matched towards a restoring profile by means of a newtonian damping, with a time scale of ten days. The restoring profile for potential temperature  $\Theta$  and salinity  $S$  of the control experiment contains shelf water masses, ranging for  $-1.9\text{ °C} \leq \Theta \leq -1.4\text{ °C}$  and  $34.30 \leq S \leq 34.65$  according to ZWIERZ (1993, profile 432), and Coastal Current water masses for the extended model domain, ranging for  $-1.9\text{ °C} \leq \Theta \leq +0.5\text{ °C}$  and  $34.30 \leq S \leq 34.65$  (ZWIERZ 1993, profiles 392 and 435; Fig. 7).

At the ocean surface, salinity varies during the year sinusoidally. In (southern) summer (at the beginning of each model year) a minimum of 34.35 is assumed, related to snow and ice melt and corresponding freshwater releases. In winter, the annual maximum of 34.55 is reached. During all seasons, temperature is restored to the surface freezing point of  $-1.9\text{ °C}$  over 30 days. In addition, the ocean surface is forced by a wind

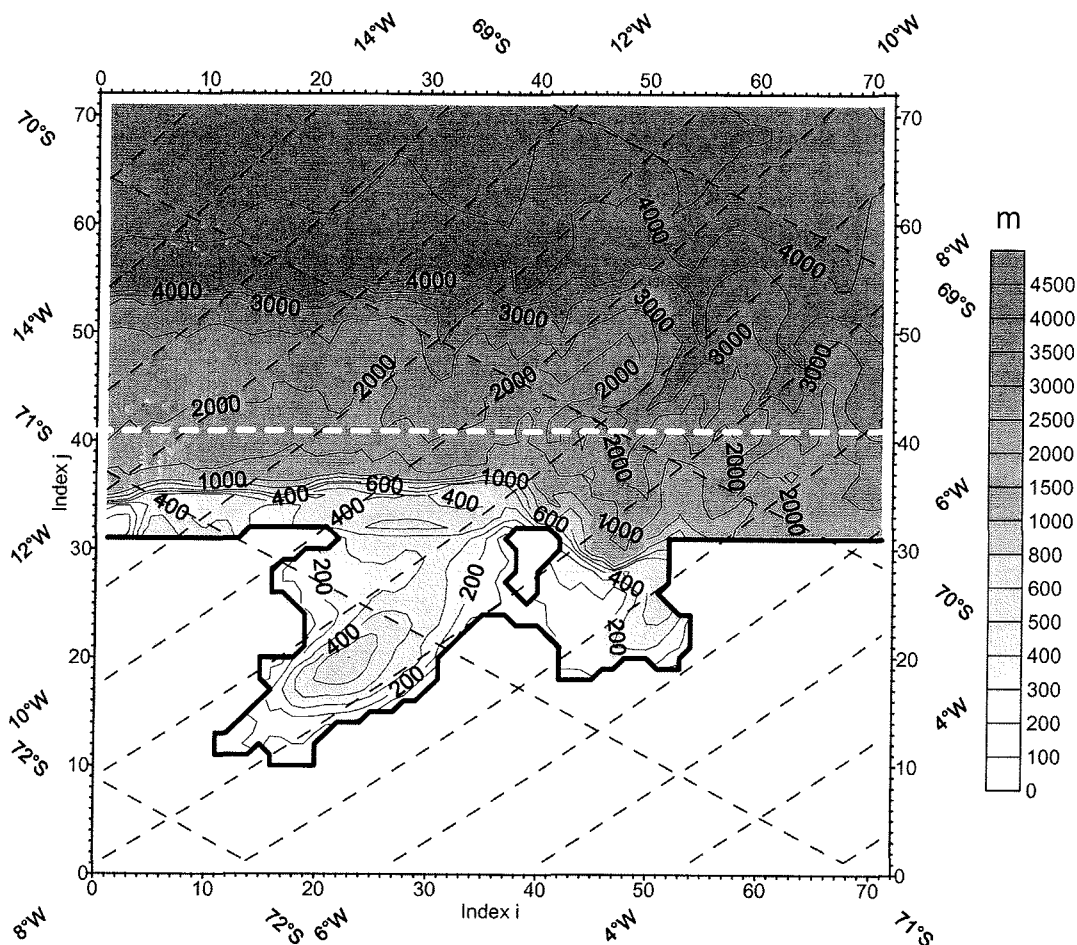


Fig. 2: Water column thickness of the extended model domain (in m). The solid line indicates the discretized grounding and coast line. Axis scales refer to the model grid indices, whereas the overlay grid represents geographic coordinates. The model domain of the control experiment comprises ice-shelf cavity and continental shelf and ends at the white dashed line ( $j = 41$ ).

Abb. 2: Wassersäulenmächtigkeit des erweiterten Modellgebiets (in m). Die durchgezogene Linie markiert die diskretisierte Aufsetz- bzw. Küstenlinie. Die Achsenbeschriftung bezeichnet Modellindizes, während das aufgelegte Gitter geographische Koordinaten darstellt. Das Modellgebiet der Standardkonfiguration umfasst die Schelfeiskaverne sowie den Kontinentalschelf und endet an der weiß gestrichelten Linie ( $j = 41$ ).

stress field which is taken from KOTTMEIER & SELLMANN (1996), representing a 6-year climatological mean.

### CONTROL EXPERIMENT

The results of the control experiment focus on the ice shelf cavity and the continental shelf. The streamfunction of the vertically integrated mass transport, basal melt rate and water mass distribution are the main parameters for analyzing ice-ocean interactions. All results refer to the western cavity part of Ekströmsisen, while the eastern part (with a much shallower water column) shows less significant ventilation and ice-shelf – ocean interactions.

### The circulation pattern

The streamfunction of the vertically integrated mass transport (Fig. 3) is a measure of the barotropic mode of ocean circulation and follows geostrophic contours in a weak stratified ocean, represented by the local water column thickness. The flow pattern in the western part of Ekströmsisen is dominated by a cyclonic (clockwise) gyre of 0.6 Sv (1 Sv =  $10^6 \text{ m}^3 \text{ s}^{-1}$ ) strength in the deep southern basin (Fig. 2). About 0.43 Sv water enter the cavity along the eastern grounding line from the open ocean. The water masses take about half a year to pass through the cavity before leaving it in the northwest. Local flow velocities range from  $0.1 \text{ m s}^{-1}$  in the open ocean and along the ice edge to  $0.4 \text{ m s}^{-1}$  near the southern grounding line, whereas the high velocities are related to ascending melt water.

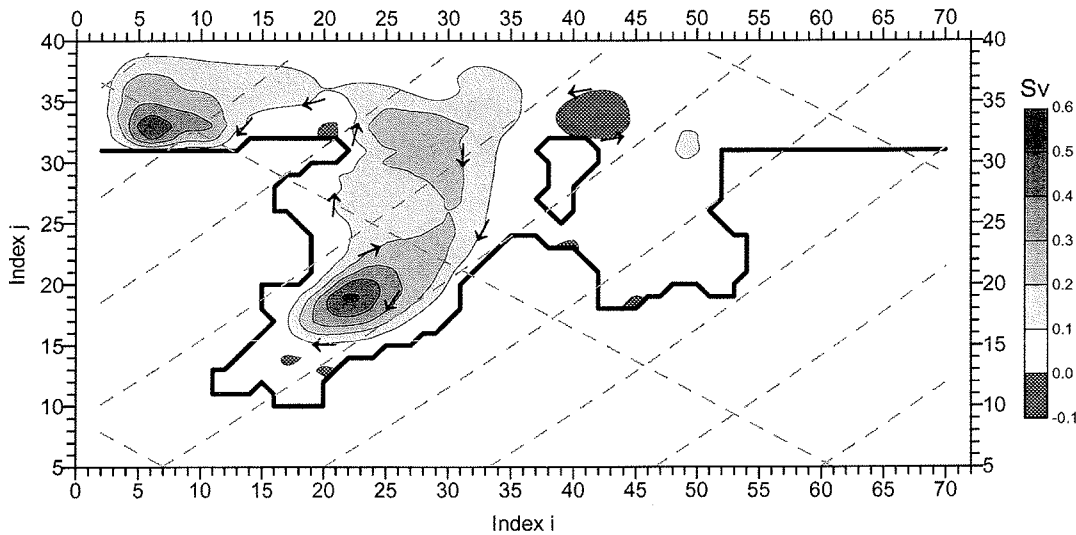


**Fig. 3:** Streamfunction of the vertically integrated mass transport of the control experiment after 8.0 model years (in Sv). Positive values represent cyclonic flow, negative anti-cyclonic flow. Arrows indicate flow direction.

**Abb. 3:** Stromfunktion des vertikal integrierten Massentransports der Standardkonfiguration nach 8,0 Modelljahren (in Sv). Positive Werte bezeichnen zyklonale Strömung, negative anti-zyklonale Strömung. Die Pfeile geben die Strömungsrichtung an.

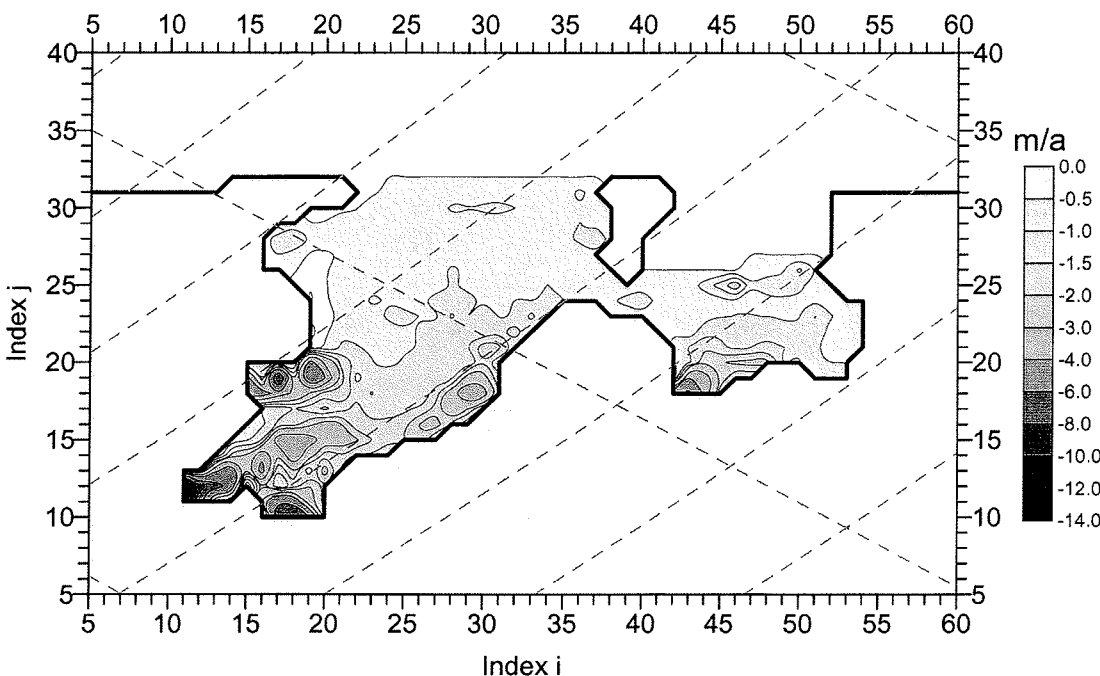


**Fig. 4:** Annual mean basal mass balance of the control experiment after 8.0 years (in  $\text{m}_{\text{ice}} \text{ a}^{-1}$ ). Negative values represent melting.

**Abb. 4:** Jahresmittel der basalen Massenbilanz der Standardkonfiguration nach 8,0 Modelljahren (in  $\text{m}_{\text{eis}} \text{ a}^{-1}$ ). Negative Werte bezeichnen Schmelzen.

### Basal mass balance

The spatial distribution of basal melting reflects the above described flow pattern in the cavity (Fig. 4). The main melting appears along the inflow region of warm water, originating from the Coastal Current, and along the grounding line in the southern part of the ice shelf, where the ice draft is greatest. At the deepest ice streams, basal melt rates exceed up to  $14 \text{ m}_{\text{ice}} \text{ a}^{-1}$ , which is related to the depression of the pressure melting point below  $-2.6 \text{ }^{\circ}\text{C}$ . The seasonal average of basal mass exchange over the whole ice shelf varies between  $0.95 \text{ m}_{\text{ice}} \text{ a}^{-1}$  (winter) and  $1.02 \text{ m}_{\text{ice}} \text{ a}^{-1}$  (summer). These variations are discussed in more detail below. The resulting mass loss due to basal melting amounts to  $7.96 \text{ Gt a}^{-1}$ , while the model does not predict any accretion of basal marine ice.

Basal melt rates and mass balances for Ekströmisen have already been estimated with two different model conceptions by SANDHÄGER & BLINDOW (2000) and KIPFSTUHL (1991), and measured at one borehole location (LAMBRECHT et al. 1995). KIPFSTUHL (1991) applied a two-dimensional massbalance model to describe the “ice pump” process in a vertical section through the cavity. Based on limited data concerning geometry and flow regime, he estimated melt rates between  $0.2 \text{ m}_{\text{ice}} \text{ a}^{-1}$  in the central ice shelf region,  $1.15 \text{ m}_{\text{ice}} \text{ a}^{-1}$  near the ice shelf front, and  $\geq 2.0 \text{ m}_{\text{ice}} \text{ a}^{-1}$  close to the grounding line. More recently, SANDHÄGER (2000) used a three-dimensional ice shelf flow model and calculated an equated massbalance for the ice shelf with an areal averaged basal mass loss of  $0.53 \text{ m}_{\text{ice}} \text{ a}^{-1}$ . The two model results agree with our study to order of magnitude and further measurements (e.g. RES measurements by SANDHÄGER & BLINDOW 2000) do not report of marine ice accumulations

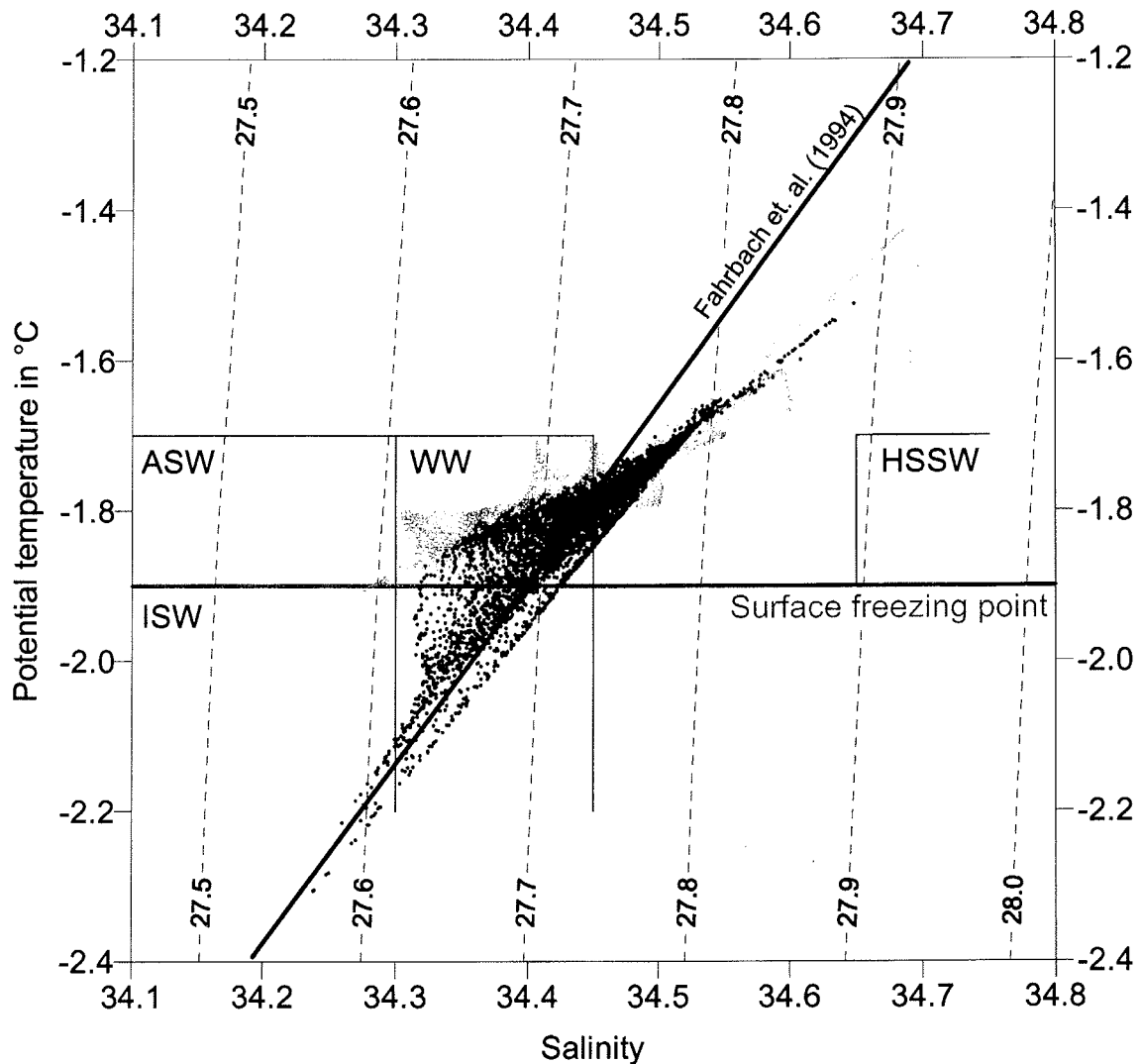


**Fig. 5:**  $\Theta$ S-diagram of the control experiment after 8.0 years. Each point represents  $\Theta$ S-properties at one grid cell located in the ice shelf cavity (black) or in the open ocean (grey). Additionally, isopycnets at surface pressure are indicated, whereas the density in  $\text{kg m}^{-3}$  results from addition of  $1000 \text{ kg m}^{-3}$ . The black line shows the theoretical modification path for water masses after FAHRBACH et al. (1994) for the EWIS region.

Abbreviations / Abkürzungen: ASW = Antarctic Surface Water; HSSW = High Salinity Shelf Water; ISW = Ice Shelf Water; WW = Winter Water.

**Abb. 5:**  $\Theta$ S-Diagramm der Standardkonfiguration nach 8,0 Modelljahren. Jeder Punkt repräsentiert  $\Theta$ S-Eigenschaften an einem Gitterpunkt innerhalb der Schelfeiskaverne (schwarz) bzw. im offenen Ozean (grau). Zusätzlich sind Isopycnen für Oberflächendruck dargestellt, wobei sich die Dichte in  $\text{kg m}^{-3}$  aus der Addition von  $1000 \text{ kg m}^{-3}$  ergibt. Die schwarze Gerade zeigt den theoretischen Modifikationspfad von Wassermassen nach FAHRBACH et al. (1994) für die EWIS-Region.

underneath Ekströmsen. More detailed comparisons, regarding local absolute values, cannot be conducted because the former massbalances contain no spatial resolution. In 1993, a hot water drilling penetrated the Ekströmsen close to Neumayer Station. From installed thermistor chains, LAMBRECHT et al. (1995) derived an average melt rate of  $0.9 \text{ m}_{\text{ice}} \text{ a}^{-1}$ . The installation of an echosounder lead to a seasonal resolution of basal melting, showing high variability. Averaged over the same period as the temperature measurements, LAMBRECHT et al. (1995) estimated  $0.93 \text{ m}_{\text{ice}} \text{ a}^{-1}$  of basal melting, but exceeding  $1.4 \text{ m}_{\text{ice}} \text{ a}^{-1}$  over 780 days. These estimations are in agreement with our simulation results, yielding  $0.5\text{-}1.0 \text{ m}_{\text{ice}} \text{ a}^{-1}$  melting for that area.

### Water masses

The water masses in the cavity and the adjacent continental shelf are primarily composed of Winter Water (WW,  $\Theta \leq -1.7 \text{ }^\circ\text{C}$ ,  $34.30 \leq S \leq 34.45$ , all water mass definitions according to GROSFELD et al. (2001)) and ISW ( $\Theta \geq -1.9 \text{ }^\circ\text{C}$ ) (Fig. 5). Directly adjacent to the ice shelf base, ISW can be identified with temperatures even below  $-2.3 \text{ }^\circ\text{C}$ . These water masses are part of the “ice pump” process and cause a rapid modification of underlying waters near the grounding line at the deep ice streams. However, only a few locations show such extreme temperatures. If the total water mass exchange between open ocean and cavity is taken into account, a mean cooling of  $0.044 \text{ }^\circ\text{C}$  of the out-flowing waters compared to the inflow has

been calculated from this simulation. The scatter plot for the control experiment reaches from the main melt regions with lowest salinity (34.25) to more saline waters in the deep open ocean (34.63). It follows the theoretical mixing line for glacial melt water with surface source waters (GADE 1979), which is given by FAHRBACH et al. (1994) for the EWIS region as  $(\Theta = -2.43 \text{ }^\circ\text{C}/\text{psu} \cdot (34.4\text{-}S) - 1.9 \text{ }^\circ\text{C})$  and indicated in Figure 5. Modification of WW to a colder fraction is a clear result from ice ocean interaction and the mixing of ISW with ambient waters in the cavity.

### EXTENDED MODEL DOMAIN

The results presented above show consistent patterns for the ice shelf cavity itself. But to allow for a more realistic representation of the interaction process between the cavity and the open ocean and to study the influence of the narrow continental shelf onto the freshwater production in the ice shelf cavity, an extension of the model domain has been performed to include a fourfold open ocean domain. The extended model grid in experiment shelf00 spans  $71 \cdot 71$  grid cells and makes it necessary to adapt a modified restoring profile at the northern boundary. These prescribed water masses are based on CTD measurements (ZWIERZ 1993) and characterized by higher temperatures on lower  $\sigma$ -levels. Both, measured and restoring water masses, are shown in the  $\Theta$ -S-diagram (Fig. 7). The streamfunction of the vertically integrated mass transport for experiment shelf00 is dominated by a large-scale cyclonic

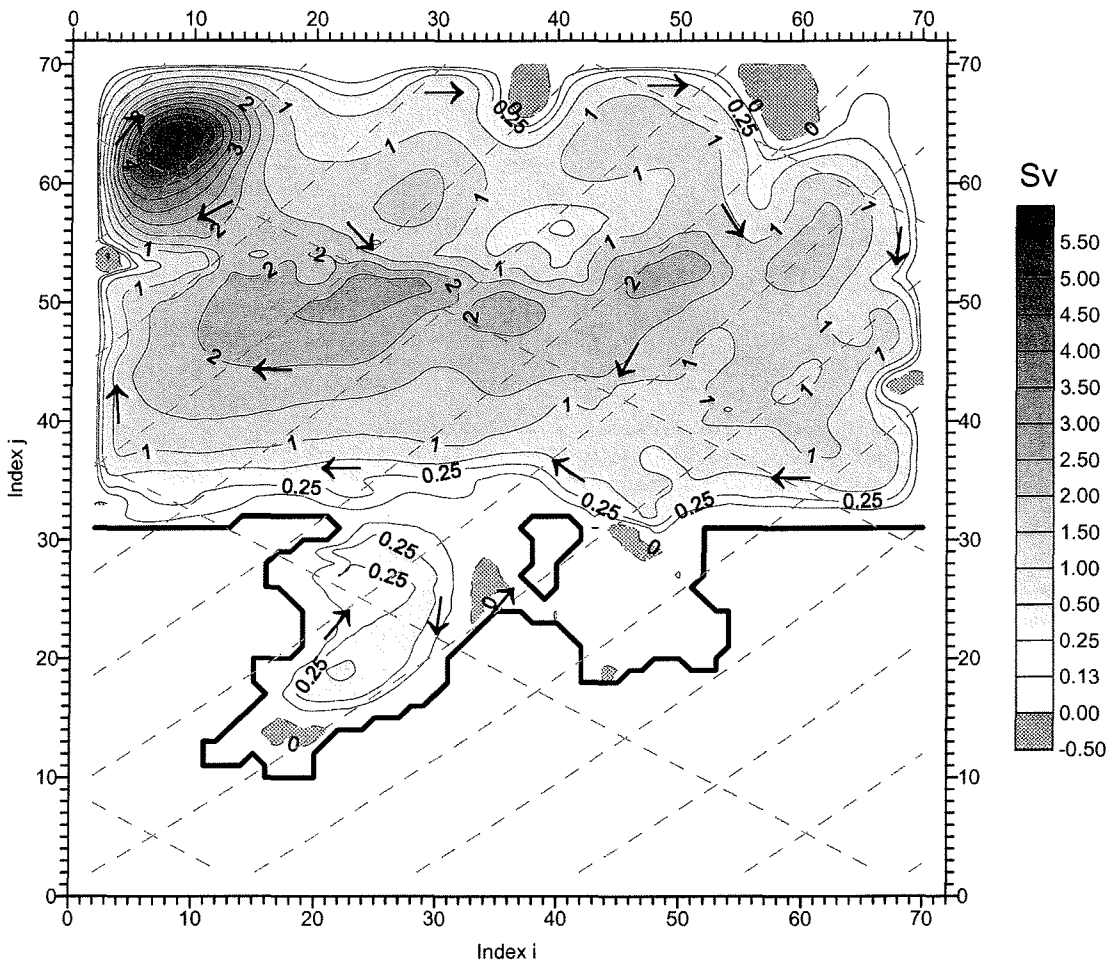


**Fig. 6:** Streamfunction of the vertically integrated mass transport of experiment shelf00 including the entire model domain after 8.0 model years (in Sv). Arrows indicate flow direction.

**Abb. 6:** Stromfunktion des vertikal integrierten Massentransports der Standardkonfiguration für Experiment shelf00 mit vergrößertem offenen Ozeanbereich nach 8.0 Modelljahren (in Sv). Die Pfeile geben die Strömungsrichtung an.

gyre, extending over the whole deep ocean (Fig. 6). This is an artificial pattern and due to closed western and eastern boundary conditions. They cause recirculation within the model domain and lead to an overestimated influence of northern water masses on the continental shelf and the ice shelf cavity. But a deliberate aspect of this recirculation is the development of a Coastal Current, which arises at the continental shelf edge with westwards flow ( $>1.0$  Sv) in front of the ice shelf. It directly interacts with the ice shelf cavity by the exchange of water masses, whereas the circulation pattern within the cavity remains similar to the control experiment and

the maximum mass transport amounts to 0.6 Sv, too.

The consideration of a larger and deeper ocean domain leads to a doubling of the annual basal mass loss within the ice-shelf cavity, while the spatial distribution (not shown here) remains similar to control experiment. The latter is certainly related to the similar circulation pattern, whereas higher melt rates are due to warmer water masses circulating through the cavity. There are two reasons for the increased amount of heat underneath Ekströmisen: on the one hand, the reinforced effect of recirculation in the open ocean leads to overestimated warm

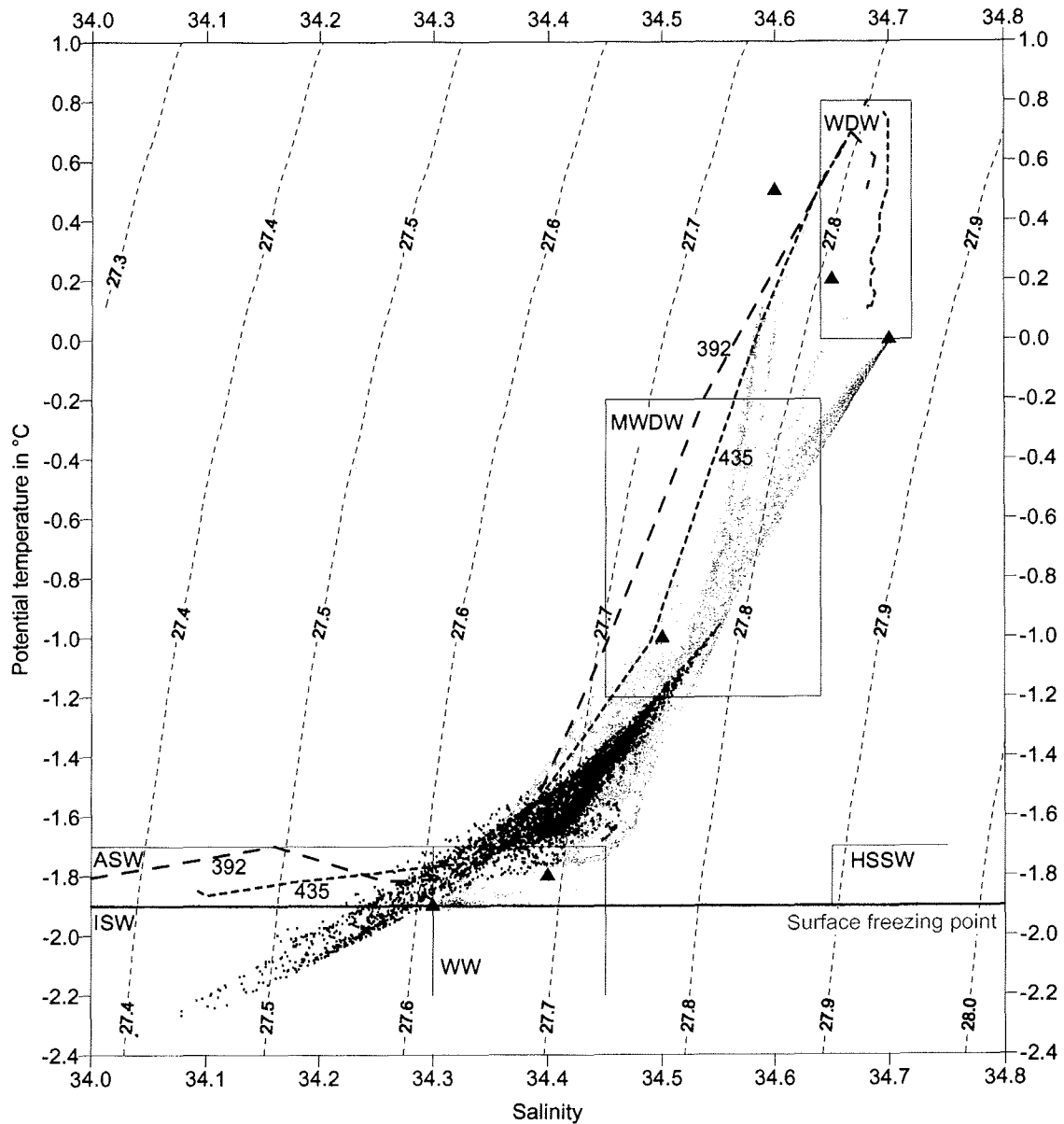


**Fig. 7:**  $\Theta$ -S-diagram of experiment shelf00 after 8.0 years. Each point represents  $\Theta$ -S-properties at one grid cell located in the ice shelf cavity (black) or in the open ocean (grey). Triangles indicate water mass properties restored at the northern boundary ( $j = 71$ ). Additionally, isopycnets at surface pressure are indicated, whereas the density in  $\text{kg m}^{-3}$  results from addition of  $1000 \text{ kg m}^{-3}$ . The dashed lines represent measured CTD profiles (No. 392 and 435) by ZWIERZ (1993).  
Abbreviations / Abkürzungen: ASW = Antarctic Surface Water; HSSW = High Salinity Shelf Water; ISW = Ice Shelf Water; MWDW = Modified Warm Deep Water; WDW = Warm Deep Water; WW = Winter Water.

**Abb. 7:**  $\Theta$ -S-Diagramm für Experiment shelf00 nach 8.0 Modelljahren. Jeder Punkt repräsentiert die  $\Theta$ -S-Eigenschaften an einem Gitterpunkt innerhalb der Schelfeiskaverne (schwarz) bzw. im offenen Ozean (grau). Dreiecke geben Wassermassen des „restoring“ am nördlichen Modellrand ( $j = 71$ ) wieder. Zusätzlich sind Isopycnen für Oberflächendruck dargestellt, wobei sich die Dichte in  $\text{kg m}^{-3}$  aus der Addition von  $1000 \text{ kg m}^{-3}$  ergibt. Die gestrichelten Linien geben gemessene CTD Profile (Nr. 392 und 435) nach ZWIERZ (1993) wieder.

water masses flowing into the ice shelf cavity. In nature, the two dominating currents, the eastward flowing part of the Weddell Gyre (north of the model area) and the Coastal Current are separated from each other and there is no mass transport towards the coast in this region. On the other hand, the narrow continental shelf represents no insurmountable obstacle for the Coastal Current to directly penetrate into the cavity. In addition, the simulation results are very sensitive towards the geometrical discretization of the narrow continental shelf, which is about 35 km wide and represented by only seven grid points in meridional direction. Hence, it is difficult to separate the two regimes ocean and cavity from each other in the numerical realization, so that warm water masses from the Coastal Current can progress unopposed into the cavity.

The impact of warmer waters entering the ice shelf cavity is also obvious from the water mass representation in the  $\Theta$ - $S$ -diagram (Fig. 7). The ISW fraction reduces and shifts to a less saline component. While the water mass in the control experiment are generally cooled through ice shelf-ocean interactions (comp. Fig. 5), the waters in this experiment are characterized by a freshwater gain (decrease in salinity) and therefore shifted to lower densities. This influences the stratification of the waters at least on the continental shelf region. A similar result was found in a coupled ice shelf-ocean model study for an ocean warming scenario by GROSFELD & SANDHÄGER (2004). Here, the dynamic response of a coupled ice-shelf – ocean system was investigated and a strong sensitivity of the ice-shelf dynamics (increased melting and change in the dynamic regime) and the water mass composition (freshening and stronger stratification) was found. Hence, flooding of ice-shelf cavities with warm water masses has direct impacts on the water mass modification on the continental shelf and the adjacent current systems.

## EXTENDED SHELF WIDTH EXPERIMENTS

To assess the importance of shelf width in more detail, further parameter studies with artificially enlarged continental shelves are performed. The influence of different discretization in respect to the basal mass balance is summarized in Table 1.

Besides the two model configurations discussed above, three further shelf configurations are simulated. Their geometry is equal to the extended model domain (shelf00) except the shelf width. To enlarge the continental shelf 2, 5, or 10 grid lines are

inserted in front of the ice edge with the same water depth as the adjacent grid lines, while the total number of lines remains 71. For this, the corresponding number of grid lines are deleted in the north.

An extension of two grid lines (shelf02, Tab. 1) reduces the average basal melt rate to an annual mean of  $1.30 \text{ m}_{\text{ice}} \text{ a}^{-1}$ , according to a reduction of basal mass loss from  $15.40 \text{ Gt a}^{-1}$  (shelf00) to  $10.34 \text{ Gt a}^{-1}$  (shelf02). This corresponds to the percentage extension of the continental shelf by 34 % and is doubtless the result of cooler water masses within the cavity, whereas the cooling has two reasons: i) warm deep water masses are more separated from the ice shelf, and it is more difficult for them to overcome the likewise broadened continental shelf and to penetrate into the cavity. ii) Due to the shallower water depth on the shelf, bottom water masses are closer to the surface where cooling (to the atmosphere) is more efficient than in the deep ocean. Hence, if the shelf width enlarges, the heat loss to the atmosphere increases and cooling of shelf waters is enhanced (FAHRBACH et al. 1994). Winter sea-ice formation in leads or polynyas becomes more efficient which yields enhanced brine releases, increasing salinity and vertical mixing of shelf waters. On the broad western shelves in the Weddell Sea, this process leads to the most saline waters (Western Shelf Waters or High Salinity Shelf Water) (CARMACK 1974).

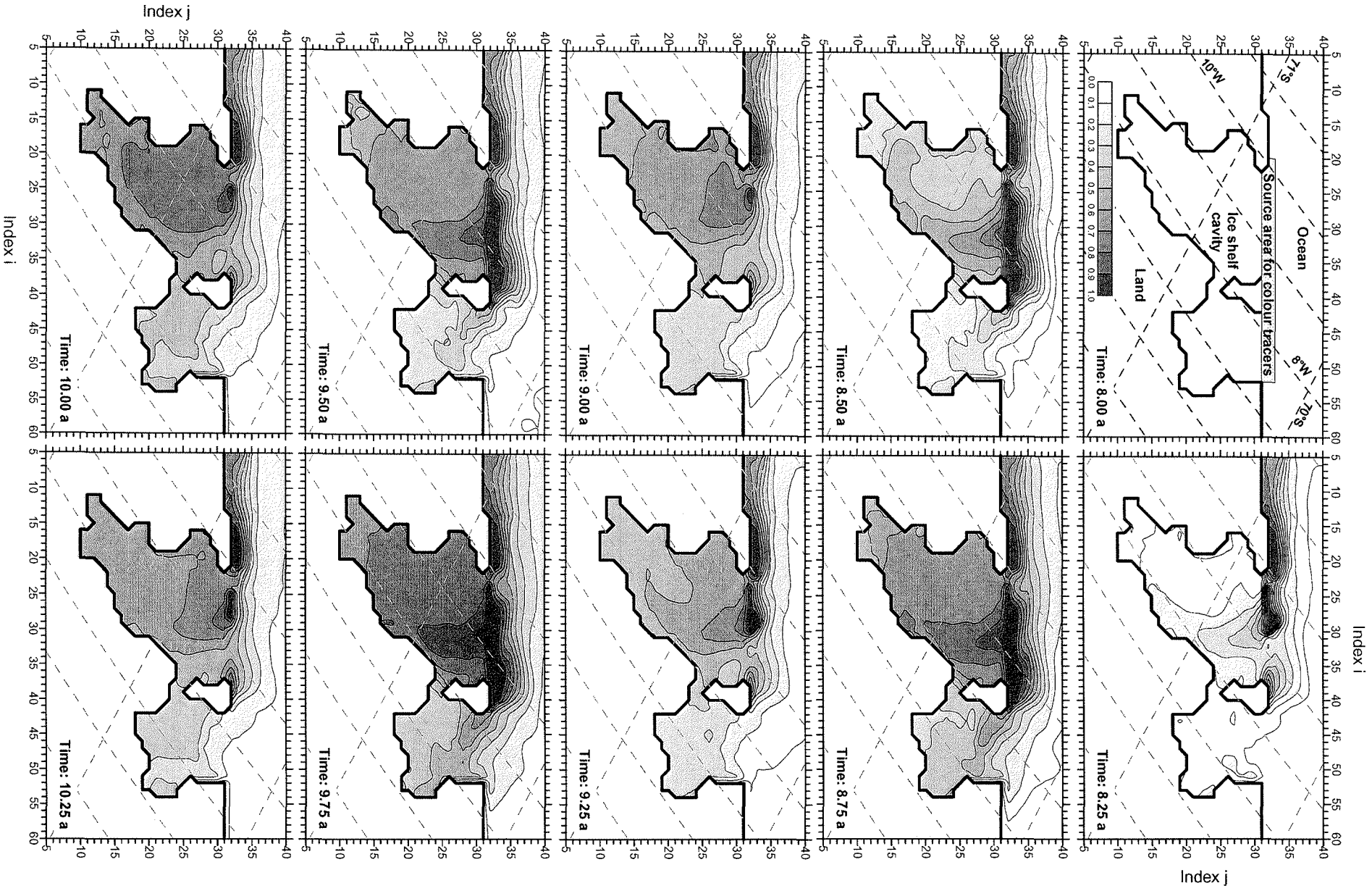
Further extensions of the continental shelf width lead to additional reductions of the basal mass balance. A total shelf width of 63 km (shelf05) reduces the minimum annual melt rate to  $1/3$  ( $0.62 \text{ m}_{\text{ice}} \text{ a}^{-1}$ ) and only  $0.52 \text{ m}_{\text{ice}} \text{ a}^{-1}$  are molten at the ice shelf base during winter times if shelf width amounts 91 km (shelf10). However, experiment shelf10 is only partly comparable to shelf02 and shelf05, because the extraordinary shelf width essentially influences the circulation pattern and not only melt rates and water mass properties.

Concluding, these studies clearly demonstrate the principle effect how shelf width affects water mass formation and composition in ice shelf cavities and the adjacent shelf. Furthermore, it underlines the importance of applying adequate spatial resolution within numerical models, to ensure correct representation of topographical features and especially of narrow continental shelves. Partially small geometrical manipulations point out how marginal variations lead to essential changes in water mass distribution on the continental shelf and in the cavity, while initialization and restoring remain unchanged.

| Experiment  | <i>control</i> | <i>shelf00</i> | <i>shelf02</i> | <i>shelf05</i> | <i>shelf10</i> |
|---|----------------|----------------|----------------|----------------|----------------|
| Shelf extension (grid cells)                                | 0              | 0              | 2              | 5              | 10             |
| Shelf width (km)  | 35             | 35             | 46             | 63             | 91             |
| Winter melt rate ( $\text{m}_{\text{ice}} \text{ a}^{-1}$ ) | 0.95           | 1.84           | 1.22           | 0.62           | 0.52           |
| Summer melt rate ( $\text{m}_{\text{ice}} \text{ a}^{-1}$ ) | 1.02           | 2.11           | 1.37           | 0.72           | 0.56           |
| Basal melting ( $\text{Gt a}^{-1}$ )                        | 7.96           | 15.40          | 10.34          | 5.66           | 4.45           |
| Mean cooling ( $^{\circ}\text{C}$ )                         | 0.044          | 0.087          | 0.057          | 0.031          | 0.025          |

Tab. 1: Dependency of basal melt rate for different model configurations after 8.0 model years. Melt rates indicate areal means.

Tab. 1: Abhängigkeit der basalen Schmelzrate für verschiedene Modellkonfigurationen nach 8,0 Modelljahren. Schmelzraten repräsentieren Flächenmittel.



## SEASONAL VARIATIONS

So far, only snapshots in time are analyzed and presented. To discuss seasonal dependencies in the process of ice – ocean interaction it is necessary to consider temporal changes in flow regime, melt rates and resulting water mass distributions. The corresponding simulations are performed based on experiment shelf00, because seasonal variations affect predominantly the surface of the open ocean. All meteorological forcing parameters (e.g. surface temperature, salinity as a parameterization for sea-ice formation, wind stress) affect the surface mixed layer and not directly the ice shelf cavity. The general flow pattern does not alter during this one-year integration with respect to circulation strength or mean trajectories. But local changes of the flow regime appear during the period, especially directly underneath and in front of the ice edge. This motivates the application of color tracers to illustrate the essential differences during an annual cycle. Therefore, passive (color) tracers are used in two studies, where the tracers are affected by advection and diffusion, but do not interact with other fluid properties, especially the equation of state. The color tracers are initialized after eight model years, when a quasi steady state of the flow regime is reached.

The first study aimed to identify different source regions of water masses, penetrating into the cavity during different seasons. After an initial input of tracers in the surface layer in front of the ice shelf, the tracer concentration increases in the cavity (Fig. 8, year 8.00-8.75), indicating that the onset of sea ice production leads to formation of saline/dense water masses which descend into the cavity. In summer, the predominating water masses have their sources in more northerly regions. They propagate below the lighter surface waters and do not contain tracers, hence the concentration reduces (Fig. 8, year 8.75-9.25). Repeating the simulation of the annual cycle over several years depicts a clear increase in tracer concentration during the winter (e.g. Fig. 8, year 9.25-9.75) and a decrease during the summer (e.g. Fig. 8, year 9.75-10.25). This corresponds well with the seasonally varying basal mass balance within the cavity, which shows increased melting in summer and lower basal melt rates in winter (Tab. 1). Here, color concentrations can directly be transferred to available heat for basal melting within the ice shelf cavity, whereas high tracer concentrations are related to cold surface water masses and low concentrations refer to warmer water from the north. This distinct annual cycle is superposed by the advection of waters through the ice-shelf cavity, which is pointed out by a delay of tracer concentrations within the western outflow compared to eastern inflow region (Section 3).

To trace the propagation of newly formed ISW, the main inflowing ice streams are chosen as the source region for a second tracer experiment (Fig. 9). As expected, ISW takes the general cyclonic flow with the main circulation (Fig. 6): ISW arises as a plume along the ice shelf bottom in the western part

of the cavity and the tracer concentration increases in easterly cavity parts shows, that modified water masses recirculate. Outflow into the open ocean takes two paths. On the one hand, it is part of the Coastal Current and advects towards the west, on the other hand upwelling in front of Ekströmisen takes place. The latter is not visible in Figure 9 (showing only the 5<sup>th</sup>  $\sigma$ -layer), but is as important as water mass spreading and leads to sea ice formation in front of the ice shelf. It is remarkable that the two southernmost ice streams are less connected to the cyclonic circulation pattern than the western ones (Fig. 9, local minimum in tracer concentration at  $i = 18, j = 17$ ). ISW from this coldest part of the cavity is slower mixed to the rest of the cavity, due to a separated gyre (see Fig. 6).

## SUMMARY AND CONCLUSIONS

Ice shelves act as coupling elements between inland ice and ocean, such that basal melt processes release cold freshwater into the global ocean. The cooling contributes to water mass modifications and in combination with salt gain on the western Weddell Sea shelves finally to the formation of deep and bottom water. Ice – ocean interaction and freshwater fluxes within the model domain, comprising Ekströmisen and the adjacent ocean, are described based on a three-dimensional thermohaline circulation model. Therefore, a high resolution (3.4 km  $\cdot$  c. 5.0 km) geometric data set is compiled, representing the two key regions, the cavity underneath Ekströmisen and the narrow continental shelf, as realistic as possible. The ocean circulation pattern within the ice-shelf cavity is dominated by a 0.6 Sv strong cyclonic gyre within the western cavity underneath Ekströmisen, such that it takes about half a year between the eastern inflow and western outflow of water masses. This exchange of heat between the open ocean and the cavity related to the ice-shelf draft of maximum 760 m is the main forcing of the ice – ocean interaction process. It leads to a seasonal varying basal mass loss between 0.95  $m_{ice} a^{-1}$  and 1.02  $m_{ice} a^{-1}$ . But in contrast to FRIS or other Antarctic ice shelves no accumulation of marine ice occurs, which agrees to previous studies and observations.

The use of passive color tracers within an extended model domain allows detailed analysis of flow patterns, especially to identify source regions of water masses entering the cavity and also the spreading of newly formed Ice Shelf Water and the associated theoretical mixing pathways. It has been found that the southernmost ice streams yield the coldest components of ISW. These do not contribute to ISW outflow as the western ice streams do, because of enhanced local recirculation. Most of the newly formed ISW along the western grounding line exits the ice front, contributing to water mass modification on the continental shelf, or is upwelling at the ice front. Color tracers along the ice front indicate that only in winter enhanced ventilation of the ice shelf cavity occurs, while in summer water masses from other locations penetrate into the

**Fig. 8:** Time dependent spreading of surface waters entering the ice shelf cavity. For this, passive color tracers are initialized at the surface in front of Ekströmisen (shaded area:  $20 \leq i \leq 52; 31 \leq j \leq 33$ ) and analyzed for the 12<sup>th</sup>  $\sigma$ -layer, located in the middle of the water column. Grey scales are equal for all plates and represent the normalized tracer concentration. Time is given in model years.

**Abb. 8:** Zeitliche Ausbreitung von Oberflächenwasser, das in die Kaverne strömt. Dazu werden passive Farbttracer an der Oberfläche vor Ekströmisen (schraffierte Fläche:  $20 \leq i \leq 52; 31 \leq j \leq 33$ ) initialisiert und in der 12.  $\sigma$ -Schicht, die sich in der Mitte der Wassersäule befindet, analysiert und dargestellt. Die Graustufen sind für alle Einzelbilder gleich und stellen die normierte Tracerkonzentration dar. Die Zeit ist in Modelljahren angegeben.

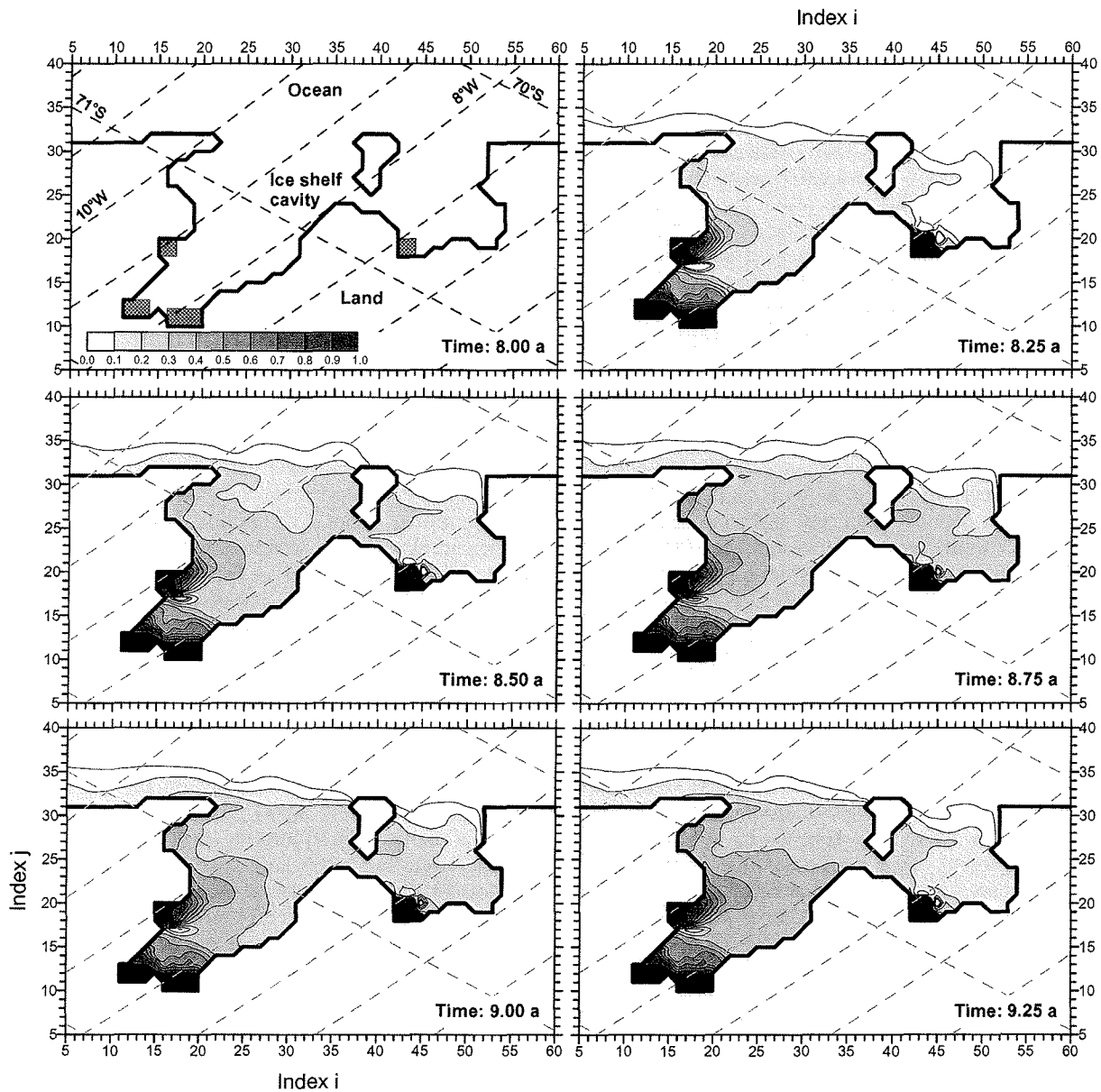


**Fig. 9:** Time dependent spreading of newly formed Ice Shelf Water. Passive color tracers are initialized at the base of main ice streams in the 5<sup>th</sup> to 7<sup>th</sup>  $\sigma$ -layer initialized and in the 5<sup>th</sup>  $\sigma$ -layer, which is the ice shelf - ocean boundary layer. Time stepping between plates is three month. Grey scales are equal for all plates and represent the normalized tracer concentration. Time is given in model years.

**Abb. 9:** Zeitliche Ausbreitung von neu gebildetem Schelfeiswasser. Dazu werden passive Tracer an den wesentlichen Einstromgletschern in der 5. bis 7.  $\sigma$ -Schicht initialisiert und in der 5.  $\sigma$ -Schicht, welche die Grenzfläche zwischen Wasser und Schelfeis ist, analysiert und dargestellt. Die Graustufen sind für alle Einzelbilder gleich und stellen die normierte Tracerkonzentration dar. Die Zeit ist in Modelljahren angegeben.

cavity. This seasonality of ventilation also determines the basal mass balance.

Furthermore, sensitivity studies with artificially enlarged shelf width show high sensitivities of the basal mass balances in the ice-shelf cavity against shelf extensions. A broadening of only 11 km (corresponding to two grid lines or 30 % of the original shelf width) leads to a decrease in basal mass loss of about 5 Gt a<sup>-1</sup> or one third. The present study, therefore, points out how sensitive freshwater flux rates in ice-shelf cavities are towards the width of the separating continental shelf and, hence, the obstruction of the source of warm water masses, here the Coastal Current. The aspect (model resolution, continental

shelf width) becomes even more important in larger scale models, with coarser resolution and less grid points representing the continental shelf. Therefore, it has to be ensured that model results are based on physical processes and topographical effects instead of discretization aspects. On the other hand, although the Ekströmisen represents one of the smaller ice-shelf regions of EWIS, it contributes to the water mass modification of the Coastal Current, which directly interacts with the ice shelf due to the narrow continental shelf. Because of this interaction process, the Coastal Current continues to cool and freshen on its westward directed flow, until it reaches the southern Weddell Sea, where it splits into two branches, one interacting with the large FRIS, the other following the

continental shelf break and participating in deep and bottom water formation when mixing with dense or cold shelf waters. Hence, the numerous small ice shelf regions of the EWIS play an important role in the process of deep-water formation, which is by now certainly underestimated.

## ACKNOWLEDGMENTS

The authors wish to thank Prof. Dr. M.A. Lange for his encouragement of this study which comprises parts of a diploma thesis carried out at the Institut für Geophysik of the Westfälische Wilhelms-Universität Münster. The work is partly funded through German CLIVAR/marine project (03F0246F3). We are grateful to Dr. H. Sandhäger for his support in processing geometrical data sets. Thorough reading and suggestions of two anonymous reviewers is greatly acknowledged.

## References

- Arakawa, A. (1966): Computational design for long-term numerical integration of the equations of fluid motion: Two-dimensional incompressible flow. Part I.- Journ. Computational Physics 1: 119-143.
- Beckmann, A. & Goosse, H. (2003): A parameterization of ice shelf-ocean interaction for climate models.- Ocean Modelling 5: 157-170.
- Beckmann, A., Hellmer, H.H. & Timmermann, R. (1999): A numerical model of the Weddell Sea: large-scale circulation and water mass distribution.- J. Geophys. Res. 104(C10): 23375-23391.
- Bryan, K. (1969): A numerical method for the study of the circulation of the world ocean.- Journ. Computational Physics 4: 347-376.
- Carmack, E. (1974): A quantitative characterization of water masses in the Weddell Sea during summer.- Deep-Sea Res. 21: 431-443.
- Cox, M.D. (1984): A primitive equation, three-dimensional model of the ocean.- Vol. 1 GDFL Ocean Group Techn. Rep., Geophys. Fluid Dynamics Lab., Princeton University.
- Fahrbach, E., Peterson, R.G., Rohardt, G., Schlosser, P. & Bayer, R. (1994): Suppression of bottom water formation in the southeastern Weddell Sea.- Deep-Sea Res. 41: 389-411.
- Foldvik, A. & Kvinge, T. (1974): Conditional instability of sea water at the freezing point.- Deep-Sea Res. 21: 169-174.
- Foldvik, A., Gammelsrød, T., Slotsvik, N. & Tørresen, T. (1985): Oceanographic conditions on the Weddell Sea shelf during the German Antarctic Expedition 1979/80.- Polar Research 3: 209-226.
- Gade, H.G. (1979): Melting of ice in sea water: a primitive model with application to the Antarctic ice shelf and icebergs.- J. Phys. Oceanography 9: 189-198.
- Gammelsrød, T., Foldvik, A., Nøst, O.A., Skagseth, Ø., Anderson, L.G., Fogelqvist, E., Olsson, K., Tanhua, T., Jones, E.P. & Østerhus, S. (1994): Distribution of water masses on the continental shelf in the southern Weddell Sea.- In: O.M. JOHANNESSEN, R.D. MUENCH & J.E. OVERLAND (eds.), The polar oceans and their role in shaping the global environment. The Nansen Centennial Volume, Geophys. Monograph Ser. 84: 159-175, Amer. Geophys. Union, Washington D.C.
- Gerdes, R. (1993): A primitive ocean circulation model using a general vertical coordinate transformation. 1. Description and testing of the model.- J. Geophys. Res. 98(C8): 14.683-14.701.
- Gerdes, R., Determann, J. & Grosfeld, K. (1999): Ocean circulation beneath Filchner-Ronne Ice Shelf from three-dimensional model results.- J. Geophys. Res. 104(C7): 15.827-15.842.
- Grosfeld, K. & Sandhäger, H. (2004): The evolution of a coupled ice shelf – ocean system under different climate states.- Global Planet. Change, Spec. Issue, Ice Sheets and Neotectonics, (in print).
- Grosfeld, K., Gerdes, R. & Determann, J. (1997): Thermohaline circulation and interaction between ice shelf cavities and the adjacent ocean.- J. Geophys. Res. 102(C7): 15.595-15.610.
- Grosfeld, K., Schröder, M., Fahrbach, E., Gerdes, R. & Mackensen, A. (2001): How iceberg calving and grounding changes the circulation and hydrography in the Filchner Ice Shelf - ocean system.- J. Geophys. Res. 106(5): 9039-9056.
- Hellmer, H.H. & Olbers, D. (1989): A two-dimensional model for the thermohaline circulation under an ice shelf.- Antarctic Sci. 1: 325-336.
- Holland, D.M., Jacobs, S.S. & Jenkins, A. (2003): Modeling Ross Sea ice shelf - ocean interaction.- Antarctic Sci. 15: 13-23.
- IFAG (1989): Ekströmisen, Topographische Karte und Satellitenbildkarte.- SS 28-30, Maßstab 1:500.000. Institut für Angewandte Geodäsie, Frankfurt am Main.
- IOC, IHO & BODC (1997): The 1997 edition of the GEBCO Digital Atlas.- Intergovernm. Oceanogr. Comm. and Internat. Hydrogr. Org. and Brit. Oceanogr. Data Centre, Birkenhead.
- Jenkins, A. (1991): A one-dimensional model of the ice shelf - ocean interaction.- J. Geophys. Res. 96(C11): 20.671-20.677.
- Jenkins, A. & Holland, D.M. (2002): A model study of ocean circulation beneath Filchner-Ronne Ice Shelf, Antarctica: implications for bottom water formation.- Geophys. Res. Lett. 29(8): 34-1-34.4, doi:10.1029/2001GL014589.
- Kipfstuhl, J. (1991): Zur Entstehung von Unterwassereis und das Wachstum und die Energiebilanz des Meereises in der Atka Bucht, Antarktis.- Berichte Polarforsch. 85: 1-88.
- Kottmeier, C. & Sellmann, L. (1996): Atmospheric and oceanic forcing of Weddell Sea ice motion.- J. Geophys. Res. 101(C9): 20.809-10.824.
- Lambrecht, A., Nixdorf, U. & Zürn, W. (1995): Ablation rates under the Ekström Ice Shelf derived from different methods.- Filchner-Ronne Ice Shelf Programme (FRISP), Report 9: 50-56.
- Lewis, E.L. & Perkin, R.G. (1986): Ice pumps and their rates.- J. Geophys. Res. 89(C10): 607-615.
- Makinson, K. (1994): The BAS hot water drill: development and current design.- Cold Regions Sci. Technol. 22: 121-132.
- Marcus, T., Kottmeier, C. & Fahrbach, E. (1998): Ice formation in coastal polynyas in the Weddell Sea and their impact on oceanic salinity.- In: M.O. JEFFRIES (ed.), Antarctic sea ice: physical processes, interactions and variability, Antarctic Res. Ser. 74: 273-292. Amer. Geophys. Union, Washington D.C.
- Mellor, G.L. (1991): An equation of state for numerical models of oceans and estuaries.- J. Atmosphere. Oceanic Technol. 8: 609-611.
- Müller, U., Sandhäger, H., Sievers, J. and Blindow, N. (1997): Glacio-kinematic analysis of ERS-1/2 SAR data of the Antarctic Ice Shelf Ekströmisen and the adjoining inland ice sheet.- Polarforschung 67 (1/2): 15-26.
- Nicholls, K.W. & Makinson, K. (1998): Ocean circulation beneath the west-ern Ronne Ice Shelf, as derived from in situ measurements of water currents and properties.- In: S.S. JACOBS & R.F. WEISS (eds.), Ocean, ice and atmosphere: Interactions at the Antarctic margin, Antarctic Res. Ser. 75: 303-318. Amer. Geophys. Union, Washington D.C.
- Nixdorf, U., Oerter, H. & Miller, H. (1994): First access to the ocean beneath Ekströmisen, Antarctica, by means of hot-water drilling.- Annals Glaciol. 20: 110-114.
- Piatkowski, U. (1987): Zoogeographische Untersuchungen und Gemeinschaftsanalysen an antarktischen Makroplankton.- Berichte Polarforsch. 34.
- Robin, G. de Q. (1979): Formation, flow and disintegration of ice shelves.- J. Glaciol. 24: 259-271.
- Robinson, A., Makinson, K. & Nicholls, K. (1994): The oceanic environment beneath the northwets Ronne Ice Shelf, Antarctica.- Annals Glaciol. 20: 386-390.
- Sandhäger, H. (2000): Quantifizierung eisdynamischer und massenhaus-haltsrelevanter Basisgrößen eines antarktischen Inlandeis-Schelfeis-Systems unter Einsatz eines numerischen Fließmodells.- Diss., Institut für Geophysik, Universität Münster.
- Sandhäger, H. & Blindow, N. (2000): Surface elevation, ice thickness, and subglacial-bedrock topography of Ekström Ice Shelf (Antarctica) and its catchment area.- Annals Glaciol. 30: 61-68.
- Schenke, H.W. (ed.) (1997): AWI Bathymetric Chart of the Weddell Sea, Antarctica, 1:3000000 at 71°S.- Alfred Wegener Institute, Bremerhaven.
- Timmermann, R., Beckmann, E. & Hellmer, H.H. (2001): The role of sea ice in the fresh water budget of the Weddell Sea.- Annals Glaciol. 33: 419-424.
- Williams, M.J.M., Grosfeld, K., Warner, R.C., Gerdes, R. & Determann, J. (2001): Ocean circulation and ice - ocean interaction beneath the Amery Ice Shelf, Antarctica.- J. Geophys. Res. 106(10): 22383-22400.
- Zwierz, M. (1993): Cruise Antarktis X/3 of RV Polarstern CTD-report.- Berichte Polarforsch. 128: 1-84.